Int. J. Electrochem. Sci., 10 **(2015)** 6135 - 6145

International Journal of
ELECTROCHEMICAL
SCIENCE
www.electrochemsci.org

Effective Enhancement of the Electrochemical Properties for $LiFePO_4$/C Cathode Materials by Lanthanum Doping

J.Z. Li[*], *S.Y. Wang, L.H. Wei, Z. Liu, Y.W. Tian*

School of Materials and Metallurgy, Northeastern University, Shenyang 110819, China
[*]E-mail: lijz@smm.neu.edu.cn

Received: 3 May 2015 / *Accepted:* 2 June 2015 / *Published:* 24 June 2015

The La-doped $LiFe_{1-x}La_{1-x}PO_4$/C material was synthesized using the low-temperature reduction-heat treatment method. The material's cathode structure and electrochemical properties were investigated using an X-ray diffraction (XRD), Fourier transform infrared spectroscopy(FTIR), scanning electron microscopy (SEM), electrochemical impedance spectroscopy (EIS), cyclic voltammetry (CV), and charge/discharge cycling. The results show that different amounts of lanthanum doping influences the structure and electrochemical properties of the material. With an increase in the doping amount in $LiFe_{1-x}La_xPO_4$/C material at x from 0 to 0.0075, the initial charge/discharge performance is visibly improved. Especially when the doping amount of La is fixed at x=0.005, $LiFe_{0.995}La_{0.005}PO_4$/C has a better performance. The initial discharge capacity presents 169.6 $mAh \cdot g^{-1}$ at 0.1C, and the capacity is retained at 167.7 $mAh \cdot g^{-1}$ after 20 cycles. Electronic conductivity, electrode reaction reversibility, structure stability, and the charge transfer process are enhanced.

Keywords: cathode material; $LiFePO_4$; doping; rare earth

1. INTRODUCTION

With more and more serious problems around energy and the environment, lithium-ion batteries are now being considered as a potential power source for energy storage. Since its introduction-in 1997 by Padhi et al.[1], $LiFePO_4$ has attracted much attention over the past two decades for powering portable electronic devices due to its low cost, high energy density, environmental benignity, and remarkable thermal stability [2-4]. Despite its advantageous characteristics, pristine $LiFePO_4$ suffers from its poor ion diffusion coefficient (10^{-14} $cm^2.s^{-1}$) and low electrical conductivity (10^{-9} $S.cm^{-1}$) [5-7], preventing its widely application in large equipments. So the following work has to be done to improve above drawbacks: (1) coating the conductive agent on the surface of $LiFePO_4$ materials to improve their conductive ability [8-9]; (2) using appropriate methods

to control morphology and particle size to reduce the lithium-ion diffusion path and electrons' transportation [10]; (3) enhancing the conductivity of $LiFePO_4$ via doping [11-13].

Among these strategies, many efforts have been focused on improving the electronic conductivity and ionic diffusion of $LiFePO_4$ for practical applications by decreasing particle size and carbon coating [2-5]. As one of these methods, doping with guest elements is the main method for reducing $LiFePO_4$ particle size and improving the properties of electrode materials [6-7]. Liu [14] et al. found that the electrochemical properties of $LiFePO_4$ materials are improved by using Nb-doping. Some reports [5-7] applied electric conductors like carbon and metal oxide coatings to $LiFePO_4$ materials, which mainly changed the electrical conductivity between particles. Chung [15] et al. synthesized $LiFePO_4$ with cationic defects and doped metal ions to improve their electronic conductivity. In a word, doping at the Fe-site, namely $LiFe_{1-x}M_xPO_4$ (M = Ni, Co, Ti, V, etc.), can have an influence on particle size, surface morphology, crystal structure, and the purity of $LiFePO_4$ materials. As a result, the different electrochemical properties of $LiFePO_4$ materials are gained. However, the amount and methods of doping with guest elements required further study. Nowadays, there are limited studies [7-16] about Fe-site doping for $LiFePO_4$ with lanthanum. In this paper, $LiFePO_4$/C composites were prepared using the low temperature reduction-heat treatment method. In addition, the $LiFePO_4$/C sample with lanthanum doping at the Fe sites was synthesized for further improving the electrochemical properties effectively. The influence of La doping on the structure, morphology, and electrochemical properties of $LiFePO_4$/C is researched in detail.

2. EXPERIMENTAL

2.1 Synthesis of $LiFe_{1-x}La_xPO_4$/C

The $LiFePO_4$ and $LiFe_{1-x}La_xPO_4$ materials were prepared via the low temperature reduction-heat treatment method, the raw materials of which were of Li_2CO_3 (97%), $FePO_4$ (98%), $NH_4H_2PO_4$ (99%), and La_2O_3 (99%). Oxalic acid and malic acid was used as the composite carbon sources in this work. The above chemicals are analytical grade. In accordance with the stoichiometric ratio of $FePO_4$, Li_2CO_3, $NH_4H_2PO_4$ and La_2O_3, they were mixed using ethylene glycol and deionized water as a solvent in a container with magnetic stirring for half an hour. The reducing agents were oxalic acid (3wt% of the starting materials) and malic acid (10wt% of the starting materials), which were added into the mixture in order to prevent Fe^{2+} oxidation to Fe^{3+}. The mixture was carried out in high-energy ball-mill at a speed of 500 r/min for about 6 hours using ethanol as a dispersant, and a kind of mushy slurry was obtained. The slurry was dried at 80℃ in a vacuum for 12 hours. Finally, the precursor was sintered at 700℃ for 14 h in N_2 gas to form the $LiFePO_4$/C materials. For comparison, the $LiFe_{1-x}La_xPO_4$/C (x=0, 0.005, 0.0075, 0.01) composites' materials were prepared using the same method.

The samples were carried out using coin cells in order to test the materials' electrochemical properties, which were assembled in an argon-filled glove box. The electrode was produced by mixing 80wt% of the active materials, 10wt% of polyvinylidene fluoride (PVDF), and 10wt% of acetylene black. After it was fully mixed to a paste and coated equably on the aluminum foil, the mixture was dried for 12 hours in the vacuum drying oven, then removed out and cut into wafers of 10mm in diameter and tablet into positive plate under 3MPa.

The cathode electrodes were prepared by mixing the active material, conducting carbon black, and binder (polyvinylidene fuoride, PVDF) at a weight ratio of 80/10/10. N-methyl-2-pyrrolidone (NMP) was added as a solvent to form homogeneous slurry. The slurry was uniformly coated on Al foil. After being dried at 120℃ for 12 h, a circular electrode was punched from the aluminum foil and used as the working electrode. Coin cells of the 2032 configuration were assembled in an argon- filled glove box. Lithium metal was used as the anode. The electrolyte consisted of a solution of 1M LiPF6 in ethylene carbonate (EC)/dimethyl carbonate (DMC) (volume ratio 1:1). A microporous polypropylene sheet (Celgard2320) was used as the separator.

2.2 Properties tests

The electrochemical capacity and cyclic characterization of the material were tested under the current densities of 0.1C, 0.5C, 1C, and 2C with a Land 2001CT battery tester, and charge-discharge tests were performed in the voltage range of 2.0 - 4.2 V (vs. Li/Li^+) using LAND-2001A systems (Wuhan, China). Cyclic voltammetry (CV) was conducted using an electrochemical workstation and a model PARSTAT 2273 (American Princeton Company) in the potential range of 2.0-4.2 V (vs. Li/Li^+) at a current density of 10 mA g^{-1} with scan rates of $0.1mVs^{-1}$. The electrochemical impedance spectrum (EIS) measurement was carried out between 0.01 Hz and 100KHz frequency. All the electrochemical measurements were performed under room temperature conditions.

ZEISS/EVO18 SEM characterized surface morphology and structure. The phase structure of the prepared samples were determined using Rigaku/UItima IV(Cukα λ=0.154056nm, 40kV, 200mA) in a 2θ range of 10° to 80°, then conducted the electrochemical impedance spectroscopy and cyclic voltammetry. The surface functional groups and structure of the samples were determined by Fourier transform infrared spectroscopy, model Nicolet 380 (American Thermo Electron). The sample was dried to a powder and mixed uniformly with a KBr (AR) mass at ratio of 1: 100, then ground and pressed into tablets under 6MPa.

3. RESULTS AND DISCUSSION

3.1 Structural and Surface Morphology

The morphologies of the samples were examined with scanning electron microscopy (SEM). Figure 1 shows the SEM image of pure $LiFePO_4/C$, and the La-doped $LiFe_{(1-x)}La_xPO_4/C$ (x=0, 0.005, 0.0075, 0.01) samples. As can be seen in Fig. 1a, particle sizes with a quite poor distribution were found in the range of approximately 0.3-4μm, and the product also presented agglomeration. In Fig. 1b, the SEM photograph of La-doped $LiFe_{(1-x)}La_xPO_4$ at x=0.005 reveals a better average particle dimension of 0.2 μm. Importantly, rare earth La led to an improved appearance with a uniform distribution. As the La ion doping amount increased from 0.0075 to 0.01, the surfaces of the products presented rough and partial agglomeration, although the particle size of the product evidently decreased. The La doping effect was the difference between the three samples. So when the La doping amount for $LiFe_{(1-x)}La_xPO_4$ is fixed at x=0.005, the product presented spherical particles, the particle

sizes were uniform, and the particles contacted closely. Theoretically, the extraction and insertion reaction of Li^+ contributed to better electronic conductivity and transmission capacity among particles [16].

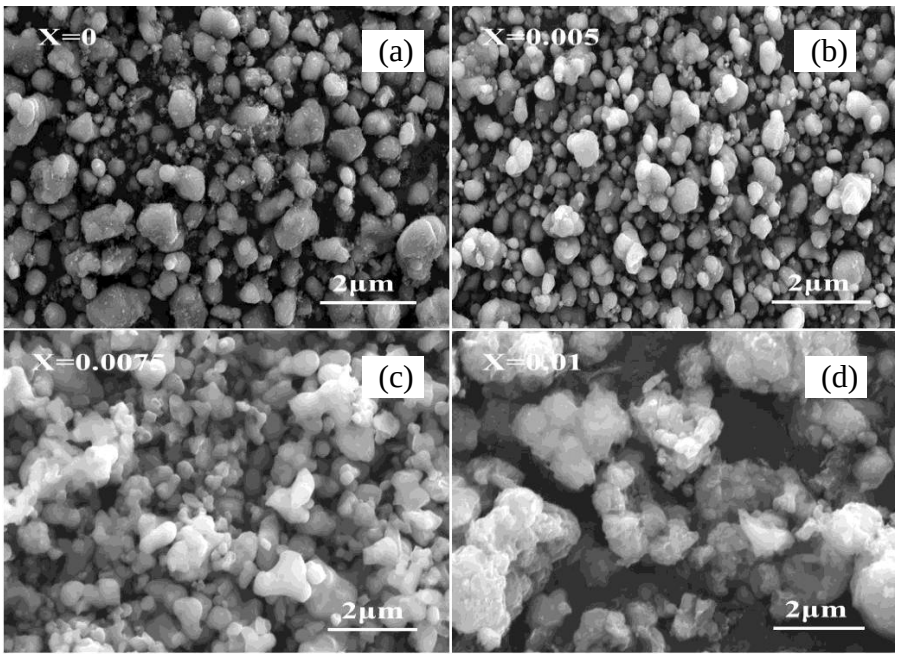

Figure 1. SEM photographs of $LiFe_{1-x}La_xPO_4/C$

Figure 2 shows the XRD patterns of $LiFe_{1-x}La_xPO_4/C$ with different amounts of the La element. Figure 2 shows the patterns of different La doping amounts compared to the standard patterns; all peaks were sharp and matched $LiFePO_4$ with olivine structure well. However, the peaks of the La element and other impurities were not found in the patterns. In addition, the peaks of graphitic carbon could not be found in the patterns, because the carbon in $LiFe_{1-x}La_xPO_4/C$ is amorphous. These results suggest that the samples have better purity in crystalline phase.

Table 1 gives the refined lattice parameters of $LiFe_{1-x}La_xPO_4/C$ (x=0, 0.005, 0.0075 and 0.01) obtained from the above XRD spectra, based on the calculation of Jade5.0 soft. As can be seen, the lattice parameters 'a' and 'b' decrease slightly, and then increase with the La doping amount, but the value of parameter 'c' decreases. This leads to lattice volume decrease. The lattice volume were reduced to 0.31%, 0.41%, and 0.75%, compared to that of the undoped material, corresponding to the amount of rare earth La doped (0.005,0.0075, and 0.01, respectively) . Lower cell volume can supply a larger channel for Li^+ transport, which makes it easier for Li^+ to extract and insert. These results can be explained by the fact that La^{3+} ions substituted Fe sites at a low doping amount and formed a complete isomorphous solid solution of $LiFe_{1-x}La_xPO_4$. In addition, the radius of La^{3+} ions (0.103nm) is smaller than that of Fe ions (0.124nm).

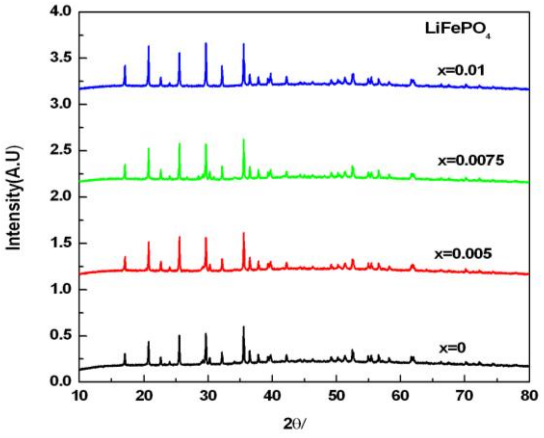

Figure 2. XRD patterns of $LiFe_{1-x}La_xPO_4/C$

Table 1. Lattice parameters of $LiFe_{1-x}La_xPO_4/C$

x in $LiFe_{1-x}La_xPO_4/C$	a (nm)	b (nm)	c (nm)	V (nm^3)
0	1.0396	0.5999	0.4711	0.2938
0.005	1.0349	0.6020	0.4702	0.2929
0.0075	1.0369	0.6034	0.4677	0.2926
0.01	1.0355	0.6029	0.4670	0.2916

Figure 3 shows the FTIR spectra of the pristine $LiFePO_4$ and $LiFe_{1-x}La_xPO_4$ (x=0, 0.005, 0.0075 and 0.01) at a range of 500 to 3500 cm^{-1}. As shown in Fig. 3a, both spectra are composed of two main peaks and five weak peaks. Stretching and bending vibrations around 3420 and 1650 cm^{-1} corresponding to O-H were observed. However, these peaks are not discussed in this paper, due to the residue amount of water with hydroxyl [19]. The peaks of 1139cm^{-1}, 1096cm^{-1}, and 1055cm^{-1} are identified at the P-O stretching vibrations, and peaks of 637cm^{-1}, 648cm^{-1}, and 475cm^{-1} correspond to the O-P-O bending vibrations, respectively, which are belong to the stretching vibrations results of the PO_4^{3-} valence bonding modes. The symmetric and asymmetric stretching peaks at 980 and 1120 cm^{-1}could be recognized. These results demonstrate that both obtained samples have a characteristic of good crystallinity as well as high purity, and the rare earth La doped $LiFe_{(1-x)}La_xPO_4$ has an insignificant effect on various PO_4^{3-} vibrational levels. However, the weak bands around 2345 and 2371 cm^{-1} are found in Fig.3b, which corresponds to the La-O stretching and bending vibrations. These suggest that the rare earth La has been doped at the $LiFePO_4/C$ materials and formed oxygen lattice defects, which help improve electrode performance.

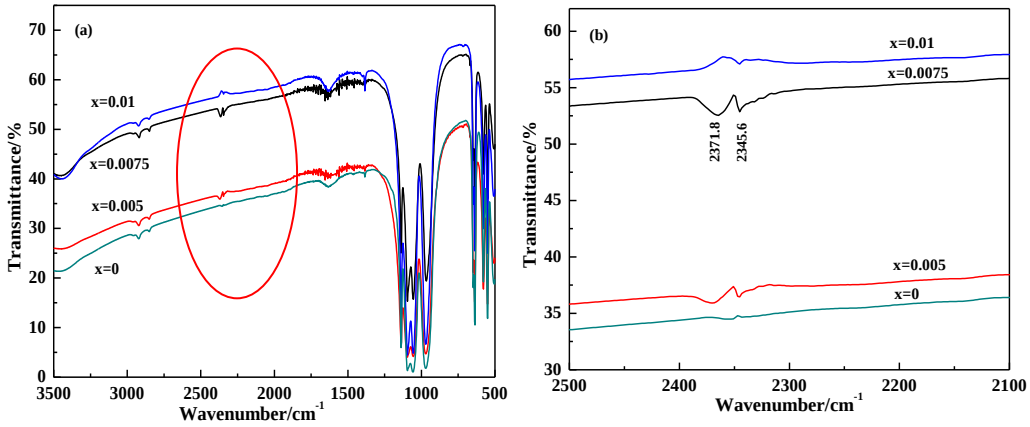

Figure 3. FTIR patterns of $LiFe_{1-x}La_xPO_4/C$: (a) photo of FTIR; (b) Partial enlarged photo of (a).

3.2 Electrochemical characterization of $LiFe_{1-x}La_xPO_4/C$

The electrochemical charge–discharge tests were first conducted to evaluate the rare earths' influence on pristine $LiFePO_4$ and $LiFe_{1-x}La_xPO_4$ (x=0, 0.005, 0.0075, and 0.01) for lithium ion batteries. Figure 4 shows the initial charge-discharge curves for different incorporations of La ions at different rates over the voltage range of 2.0-4.2 V. As shown in Fig. 4, both samples have typical flat voltage plateaus at around 3.4 V, which may be attributed to the two-phase reaction of $LiFePO_4$ and $FePO_4$. However, compared to the non-doped $LiFePO_4/C$ sample, the La doped $LiFe_{1-x}La_xPO_4$ presents the wider voltage plateau with a smaller polarization part, suggesting that the doped sample has better reaction kinetics. In addition, significant improvement of the initial charge-discharge capacity was found. The $LiFe_{0.995}La_{0.005}PO_4/C$ sample exhibited discharge capacities of 169.6, 162.5, 152.5, 140.1, and 93.6 $mAh \cdot g^{-1}$ at 0.1C, 0.2C, 0.5C, 1.0C, and 2.0C, respectively, while the $LiFePO_4/C$ sample with La doping delivered discharge capacities of 158.6, 152.4, 143.5, 132.6, and 90.2mAh g^{-1}. The results demonstrate that La doping has a significant effect on the discharge capacities of $LiFe_{1-x}La_xPO_4/C$ at different current rates. This is because the La element induces the properties of $LiFe_{0.995}La_{0.005}PO_4/C$ samples, such as homogeneous, smaller particle sizes, and large surface areas, which cause more reactions and a shorter distance for fast Li-ion diffusion in the redox reaction process. Similar phenomena are found in other studies using positive ion doping [17]. But increasing the doped amount of La reduced the initial charge-discharge capacity, as shown in Fig. 4. It is likely that the addition of La contributed to the formation of smaller $LiFe_{1-x}La_xPO_4/C$ particle sizes, and then agglomeration was gradually generated. This inhibited or increased the presence of the unstable phase, leading to lower electrochemical activity.

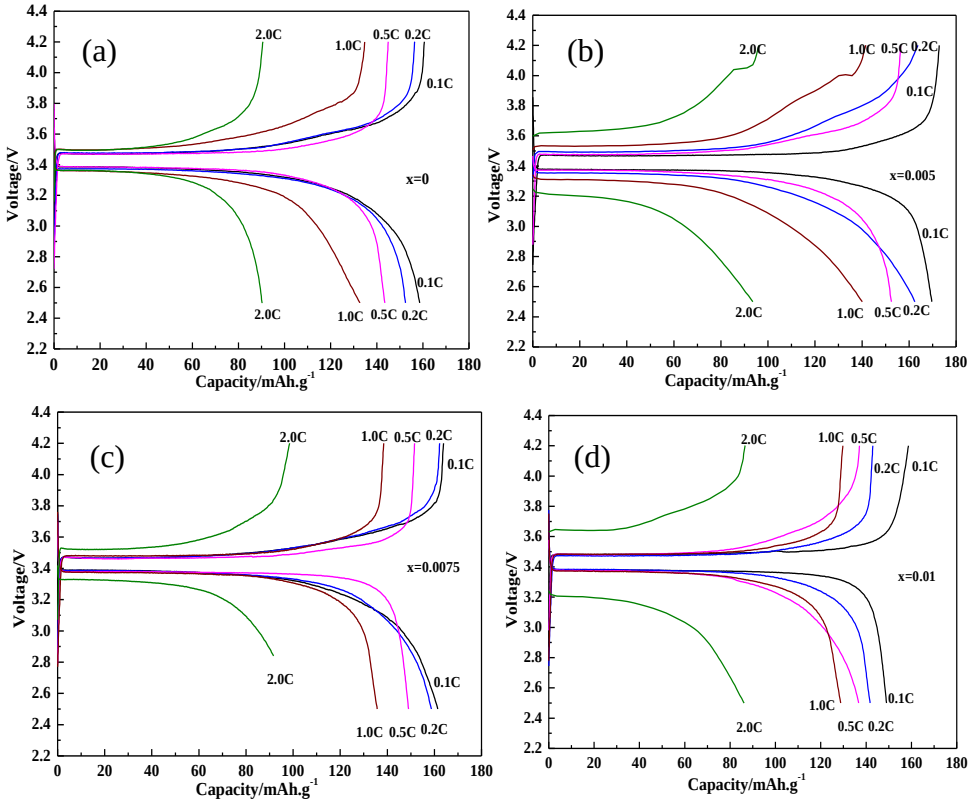

Figure 4. The first charge and discharge curves of $LiFe_{1-x}La_xPO_4/C$ at different rates: (a) $LiFePO_4/C$; (b) $LiFe_{0.995}La_{0.005}PO_4/C$; (c) $LiFe_{0.9925}La_{0.0075}PO_4/C$; (d) $LiFe_{0.99}La_{0.01}PO_4/C$;

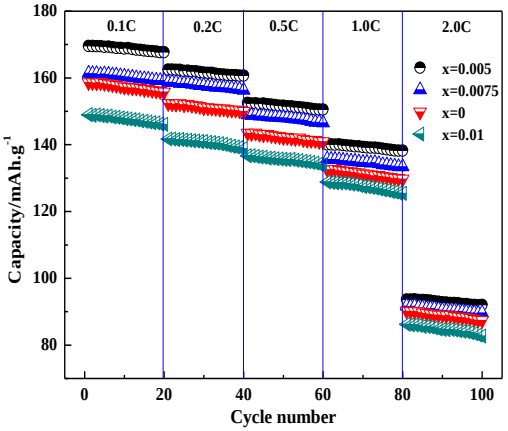

Figure 5. The cycle property of $LiFe_{1-x}La_xPO_4/C$ at different rates

Figure 5 shows the cycle performance of pristine $LiFePO_4$ and $LiFe_{1-x}La_xPO_4$ (x=0, 0.005, 0.0075 and 0.01). The cells were first discharged at 0.1 C, 0.5C and 0.2C rates, and then discharged at 1.0 C and 2.0 C rates, respectively. All discharged tests were remained at 20 cycles. For the non-doped $LiFePO_4/C$ and the doped $LiFe_{1-x}La_xPO_4/C$ materials, there was a minor change in the capacity loss at 0.1 C rates. With increasing the discharge rates, the reversible capacities of pristine $LiFePO_4$ visibly decreased. When the rate was fixed at 0.5 C rates, the capacity loss of pristine $LiFePO_4$ reached 1.3% after 20 cycles. Unlike that of pristine $LiFePO_4$, the La-doped $LiFePO_4$ presented a clearly steady cycle properties at high current rates. As increasing the rate to 2 C, the capacity of the $LiFe_{0.995}La_{0.005}PO_4$

cathode had a loss of only 0.6% after 20 cycles. With an increased La doped amount in the doped $LiFe_{1-x}La_xPO_4$ material, the capacity loss was still found during the cycle, and the extent of the decline in capacity was obviously restrained. But when the La doped amount reached 0.01, the discharge capacity of $LiFe_{1-x}La_xPO_4$ presented a capacity fading of 3.2%. It has come to light that the cycle performance and capacity of $LiFePO_4$/C materials decreases rapidly at high current densities, which is mainly attributed to their low electronic conductivity and the rapid increase of the charge transfer resistance at high rates; excess La doping of $LiFePO_4$ materials may induce a relatively lower particle size and agglomeration.

Figure 6 depicts the effect of La doping on the electrochemical properties of $LiFe_{1-x}La_xPO_4$ (x=0, 0.005, 0.0075 and 0.01) materials, further investigated by cyclic voltammetry (CV) in the voltage range of 2.0-4.5V at a scanning rate of $0.1mV.s^{-1}$. As to both samples, CV curves have a pair oxidation/reduction peaks, corresponding to the Fe^{2+}/Fe^{3+} redox reaction. The anodic peaks of $LiFePO_4$/C, $LiFe_{0.995}La_{0.005}PO_4$/C, $LiFe_{0.9925}La_{0.0075}PO_4$/C, and $LiFe_{0.99}La_{0.01}PO_4$/C appear at 3.60V, 3.51 V, 3.57V, and 3.64V, respectively, and their corresponding reduction peaks are at 3.30V, 3.37V, 3.28V, and 3.31V. The potential differences are determined to 0.30V, 0.14V, 0.19V and 0.33V, respectively. Clearly observed the $LiFe_{0.995}La_{0.005}PO_4$/C sample, the CV exhibits much higher oxidation and reduction peaks current with smaller potential separation. Sharper oxidation/reduction peaks with smaller potential separation demonstrates more wide channels for Li^+ deinsertion-insertion and finer reversibility for battery materials during the charge-discharge process [18]. According to these datas, we can conclude that La-doping efficiently reduces the polarization of active materials. In addition, the results suggest that La-doping stabilizes the crystal structure, improving the electrochemical performance of $LiFePO_4$/C materials.

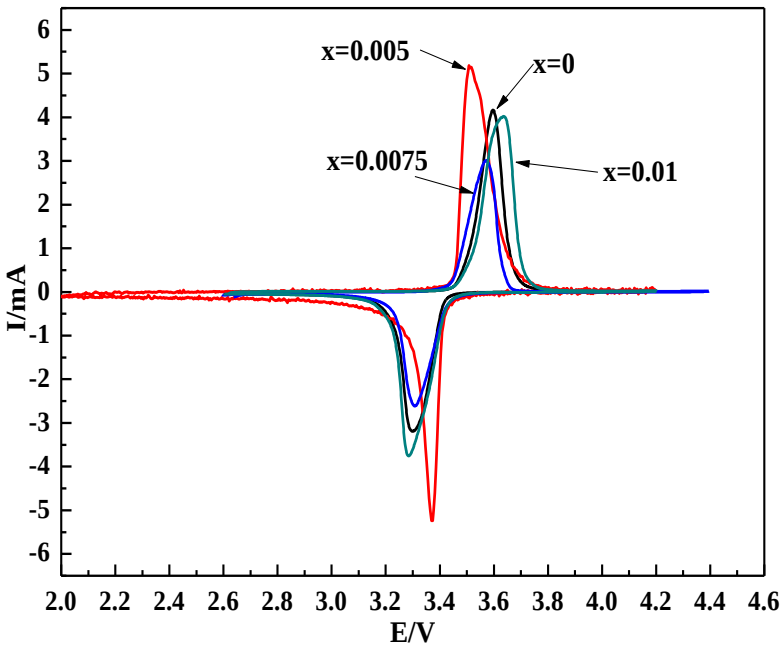

Figure 6. Cyclic voltammograms of $LiFe_{1-x}La_xPO_4$/C

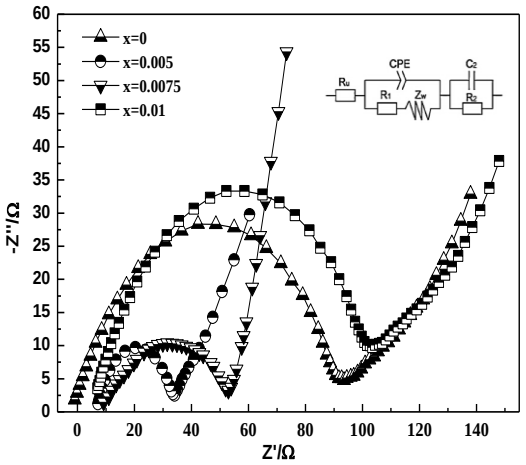

Figure 7. EIS spectra of $LiFe_{1-x}La_xPO_4/C$

Table 2. Impedance parameters calculated from the equivalent circuits for $LiFe_{1-x}La_xPO_4$ (x=0, 0.005, 0.0075 and 0.01)

Samples	$R_w(\Omega)$	$R_1(\Omega)$	$R_2(\Omega)$	$i^0(mA.cm^{-2})$
x=0	0.854	35.17	7.36	0.767
x=0.005	1.322	41.11	3.54	0.621
x=0.0075	0.721	76.93	5.11	0.412
x=0.01	0.932	65.3	6.44	0.543

In order to deeply study the influence of La doping on improving electrochemical properties, the results of electrochemical impedance spectra for pristine $LiFePO_4$ and $LiFe_{1-x}La_xPO_4$ (x=0, 0.005, 0.0075 and 0.01) are shown in Fig. 7. The impedance spectra with different La doping consist of capacitive loops at the high frequency and a straight line at the low frequency. The corresponding equivalent circuit model is inset in Fig. 7. As can be seen in Fig. 7, the Z_{re} at high-frequency is considered to the Ohmic resistance (R_w), which is attributed to the electrolyte resistance and other physical resistances. The capacitive loops in high frequencies have a relation with the Li-ion migration resistance (R_1) between the cathode and electrolyte interface [19-20]. The straight line in the low frequencies corresponds to the Warburg impedance (Z_w). The Z_w represents Li^+ ion diffusion in the $LiFePO_4$ particles. In addition, the double layer capacitance was considered to a constant phase element (CPE). The surface polarization resistance (R_2) and surface capacitance (C_2) are also represented in the simplified equivalent circuit model. Calculations from computer simulations using the Zview 2.0 software, R_w, R_1, R_2, and exchange current density values are shown in Table 2. One can see the significant decrease of the charge transfer resistance (R_1) of La-doping at $LiFe_{0.995}La_{0.005}PO_4/C$ in comparison to that of the pristine $LiFePO_4/C$ material. The reason for this is that the $LiFe_{0.995}La_{0.005}PO_4/C$ with conducting network structure provides more wide channels for the transfer of charges in the cathode electrode, leading to solvation ability and polarizability improvement. From the above CV and EIS results, the La-doping mixed conducting network into the $LiFe_{0.995}La_{0.005}PO_4/C$ material could remarkably enhance electronic conductivity, electrode reaction reversibility, and the

charge transfer process, which conduct improving properties of La-doping at the $LiFe_{0.995}La_{0.005}PO_4/C$ electrode.

4. CONCLUSIONS

Lanthanum (La) doped $LiFePO_4/C$ cathode materials were prepared by the low temperature reduction-heat treatment method, and the effect of La doping on electrochemical properties and the structure of $LiFePO_4/C$ was investigated to improve the properties of $LiFePO_4/C$ cathode materials, using XRD, FTIR, SEM and electrochemical tests. The results show that La doping improves the discharge-specific capability of cathode materials and decreases charge transfer resistance. In addition, the existence of La stabilizes the crystal structure and reducing the homogeneous particles' size, and improves ionic diffusion during both the charge and discharge processes. When the La doping amount of the $LiFe_{1-x}La_xPO_4/C$ material is fixed at x=0.005, homogeneous particles with a smaller size of cathode material are observed from the SEM results. According to electrochemical tests, the $LiFe_{0.995}La_{0.005}PO_4/C$ sample exhibits superior electrochemical performance with specific capacities of 169.6, 162.5, 152.5, 140.1, and 93.6 $mAh \cdot g^{-1}$ at 0.1C, 0.2C, 0.5C, 1.0C, and 2.0C, respectively, in comparison with that of other $LiFePO_4/C$ samples. From the XRD and FTIR results, La has been successfully embedded in the $LiFePO_4/C$ materials.

ACKNOWLEDGEMENTS
This work was financially supported by the National Natural Science Foundation of China (51374053) and the Special Fund for Basic Scientific Research of Central Colleges (N130502002).

References

1. J.L. Li, J.H. Wu, Y. Wang, G.B. Liu, C. Chen and H. Liu, *Mater. Lett.*, 136 (2014) 282.
2. W.J. Fergus, *J. Power Sources*, 195(2010) 939.
3. S.X. Liu and H. B. Wang, *Mater. Lett.*, 122 (2014) 151.
4. X.H. Liu, X.Y. Chen, Z.W. Zhao and X.X. Liang, *Hydrometallurgy*, 146 (2014) 24.
5. D. Ziolkowska, K.P. Korona, B. Hamankiewicz, S.H. Wu, M.S. Chen, J.B. Jasinski and M. Kaminska, *Electrochim. Acta*, 108 (2013) 532.
6. L.X. Liao, X.Q. Cheng, Y.L. Ma, P.J. Zuo, W. Fang, G.P. Yin and Y.Z. Gao, *Electrochim. Acta*, 87 (2013) 466.
7. R. Trócoli, S. Franger, M. Cruz, J. Morales and J. Santos-Pẽna, *Electrochim. Acta*, 135 (2014) 558.
8. Y. Cui, X.L. Zhao and R.S. Guo, *J. Alloy. Compd.*, 490 (2010) 236.
9. Y.Y. Liu and C.B. Cao, *Electrochim. Acta*, 55 (2010) 4694.
10. L.J. Li, X.H. Li and Z.X. Wang, *J. Alloy. Compd.*, 497(2010) 176.
11. Y.R. Wang, Y.F. Yang and X. Hu, *J. Alloy. Compd.*, 481 (2009) 590.
12. H.B. Shu, X.Y. Wang, W.C. Wen, Q.Q. Liang, X.K. Yang, Q.L. Wei, B.N. Hu, L. Liu, X. Liu, Y.F. Song, M. Zho, Y.S. Bai, L.L. Jiang, M.F. Chen, S.Y. Yang, J.L. Tan, Y.Q. Liao and H.M. Jiang, *Electrochim. Acta*, 89 (2013) 479.
13. H.F. Yue, Z.J. Wu and L.S. Li, *J. Alloy. Compd.*, 583 (2014) 1.
14. Y. Liu, J.C. Shi and Z.P. Gou, *J. Alloy. Compd.*, 194 (2009) 786.
15. S.Y. Chung, J.T. Bloking and Y.M. Chiang, *Nat. Mater.*, 1(2002) 123.
16. L. Wang, C.M. Jiao, G.C. Liang, N.N. Zhao, Y.M. Wang and L.C. Li, *J. Rare. Earth.*, 32(2014)

895.
17. L.F. Li, S.C. Han, C.L. Fan, Y.M. Bai and K.H. Zhang, *Mater. Lett.*, 108 (2013) 156.
18. M. Talebi-Esfandarani and O. Savadogo, *Solid State Ionics*, 261 (2014) 81.
19. G. Wu, Y.K. Zhou and Z.P. Shao, *Appl. Surf. Sci.*, 283 (2013) 999.
20. J.Z. Li, X.L. Sun, Y.W. Tian and Y. Zhao, *Int. J. Electrochem. Sci.*, 8 (2013) 6553.